C. R. Physique 15 (2014) 48–57

Contents lists available at ScienceDirect

Comptes Rendus Physique

www.sciencedirect.com

Quasicrystals / Quasicristaux

Surfaces of quasicrystals

Les surfaces des quasicristaux

Julian Ledieu *, Vincent Fournée

Institut Jean-Lamour, UMR 7198 CNRS, Université de Lorraine, parc de Saurupt, CS 50840, 54011 Nancy, France

ARTICLE INFO

Article history:
Available online 4 December 2013

Keywords:
Quasicrystal
Surface science
Thin film growth

Mots-clés :
Quasicristaux
Science des surfaces
Films minces

ABSTRACT

The remarkable surface properties of quasicrystals have motivated extensive investigations of their intrinsic atomic and electronic structures. In this article, we summarize some of the main conclusions obtained so far. We also describe adsorption experiments where quasiperiodic surfaces are used as templates to grow thin films with novel structures. Finally we discuss some of their useful properties of current interest.

RÉSUMÉ

Les propriétés de surface remarquables des quasicristaux ont été à l'origine de nombreuses études concernant leurs structures atomiques et électroniques intrinsèques. Dans cet article, nous présentons un résumé des principales conclusions obtenues jusqu'à maintenant. Nous décrivons également des expériences d'adsorption dans lesquelles des surfaces quasipériodiques sont utilisées comme patron pour la croissance de films minces de structures nouvelles. Finalement, nous discutons de quelques-unes des propriétés de surface qui sont actuellement étudiées pour d'éventuelles applications.

1. Introduction

At the end of the 18th century, it was realized that the shape of natural crystals and the angles between exposed facets reflected their internal symmetry. Similarly, faceted samples have been observed in quasicrystalline materials grown in the laboratory. For example, self-flux-grown samples of decagonal quasicrystalline phases typically appear as ten-sided column extending along the ten-fold symmetry axis. Icosahedral phases tend to adopt dodecahedral shapes with pentagonal facets reflecting their five-fold symmetry. However, quasicrystal grains with more complex shapes have also been observed, exposing not only five-fold but also two-fold and three-fold facets. The question then arose about what should be the true equilibrium shape of quasicrystals. It might differ from the shape of as-grown samples because crystal growth does not always occur in perfect equilibrium conditions.

An early theoretical study predicted a completely faceted shape for 2D and 3D quasicrystals [1]. The Wulff construction yielded a decagonal shape in 2D and a great rhombicosidodecahedron in 3D, a polyhedron possessing five-fold, three-fold and two-fold symmetry axes. A representation of this polyhedron is shown in Fig. 1. It reproduces well the shape of faceted microvoids that are formed through vacancy condensation upon long-term annealing of bulk samples. The shape of these

* Corresponding author.
E-mail addresses: julian.ledieu@univ-lorraine.fr (J. Ledieu), vincent.fournee@univ-lorraine.fr (V. Fournée).

1631-0705/$ – see front matter
http://dx.doi.org/10.1016/j.crhy.2013.09.009

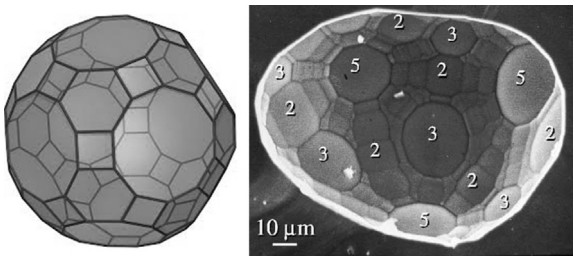

Fig. 1. (Left) A representation of the great rhombicosidodecahedron. (Right) Scanning electron microscopy image of a microvoid observed at the fracture surface of a long-term annealed sample of the icosahedral Al–Pd–Mn quasicrystal. Adapted from Ref. [3].

microvoids revealed by fracture surfaces is considered to reflect the equilibrium quasicrystal shape. The relative area of the two-, three- and five-fold facets are found to be nearly equal, indicating very small anisotropy of the surface energies for icosahedral phases [2,3]. Decagonal quasicrystals usually exhibit a pronounced anisotropy of their physical properties within the quasiperiodic planes and along the periodic direction. However, no similar observation of faceted microvoids has been reported for this class of quasicrystals, and therefore it is not possible to conclude about surface energy anisotropy in this case. However, we will see later that faceting has been observed for some two-fold surfaces of decagonal phase, a fact that might indicate a lower stability compared to other low-index surfaces of the same phase.

Absolute values of the surface energies are not known for quasicrystals. However, extensive studies of the useful surface properties of quasicrystals by Dubois et al. have led to estimated values of the surface energy for Al-based quasicrystals that are surprisingly low, on the order of 0.5 to 0.8 J/m^2, i.e. lower than the surface energy of its constitutive elements [4]. These observations as well as other studies revealing interesting surface properties like low friction and adhesion have motivated extensive investigations of clean surfaces of quasicrystals. Such investigations must be performed in ultra-high-vacuum conditions (P in the low 10^{-10} mbar range) to avoid any surface contamination. Then, it is possible to determine the surface atomic and electronic structures and compare them with bulk structural models. In the following, we summarize some of the main results obtained on well-investigated surfaces. Then we describe other experiments where clean quasicrystalline surfaces are used as a substrate for adsorption studies, with the idea to grow thin films with novel structures. Finally, we describe some of the surface properties that have attracted interest for potential applications.

2. Atomic and electronic structures of clean surfaces

2.1. The five-fold surface of the icosahedral Al–Pd–Mn quasicrystal

The five-fold surface of the icosahedral Al–Pd–Mn quasicrystal remains the most studied aperiodic surface up to today. The main reasons behind so much attention lie in the initial availability of large-enough samples for surface science investigations. The intellectual challenge to understand the atomic arrangement on a five-fold surface along with the aesthetic nature of the material has added to the motivation. One of the major hurdles in studying the i-$Al_{70}Pd_{21}Mn_9$ surface has been surface preparation. The preparation method can lead to depletion or enrichment of one element at the surface, hence shifting the overall composition away from the narrow icosahedral quasicrystal region. Upon sputtering, aluminium (the lightest element) depletion results in the formation of a crystalline β-AlPd phase exhibiting a CsCl-type structure [5–8]. When the sputtered surface is annealed at 700 K, the crystalline structure (with bcc (113)-oriented domains) is preserved. Ultra-violet photoemission spectroscopy (UPS) indicates a surface with a metallic character [8]. Sputtering the i-$Al_{70}Pd_{21}Mn_9$ surface while maintained in the range 500–700 K produces a decagonal epilayer with an $Al_{22}Pd_{56}Mn_{22}$ composition different from that of the bulk decagonal quasicrystal [9]. In all cases, subsequent annealing treatments above 700 K restore the quasicrystal composition, the five-fold symmetric low-energy electron diffraction (LEED) pattern, and the opening of a pseudogap in the electronic density of states (DOS) at the Fermi level [5–9].

Annealing the i-$Al_{70}Pd_{21}Mn_9$ surface between 700 K and 930 K produces different topographies, as observed using scanning tunneling microscopy (STM) [10]. In the range 700–830 K, the surface is rough and exhibits cluster-like protrusions. The surface structure of the five-fold surface is then comparable to the one obtained after a cleavage of the sample followed by heat treatment [11]. Micrometer-sized atomically flat terraces can be produced by sputtering and annealing cycles between 830 and 930 K for several hours [12]. The terraces are separated by two main step heights, namely $L = 6.6$ Å and $M = 4.1$ Å, distributed according to the Fibonacci sequence ($\ldots LMLLMLMLLM \ldots$) as initially presented by Schaub et al. [13]. The L/M step height ratio approaches, within the accuracy of the measurements, the golden ratio τ. An additional smaller step $S(\approx L - M = 2.4$ Å) has been also reported, but it appears less frequently [14]. As for crystalline systems, an analysis of the large-scale roughness of the steps indicates that the step height diffusivity decreases with increasing quasicrystal step heights [15]. Annealing the five-fold i-$Al_{70}Pd_{21}Mn_9$ quasicrystal surface at higher temperatures (close to the melting point) results eventually in the decomposition of the surface and the formation of a new phase. The unit cell parameters measured by STM combined with the composition ($Al_{75}Pd_6Mn_{19}$) determined by scanning electron microscopy are consistent with an Al_3Mn orthorhombic phase, assuming Pd substitution on Mn sites [16].

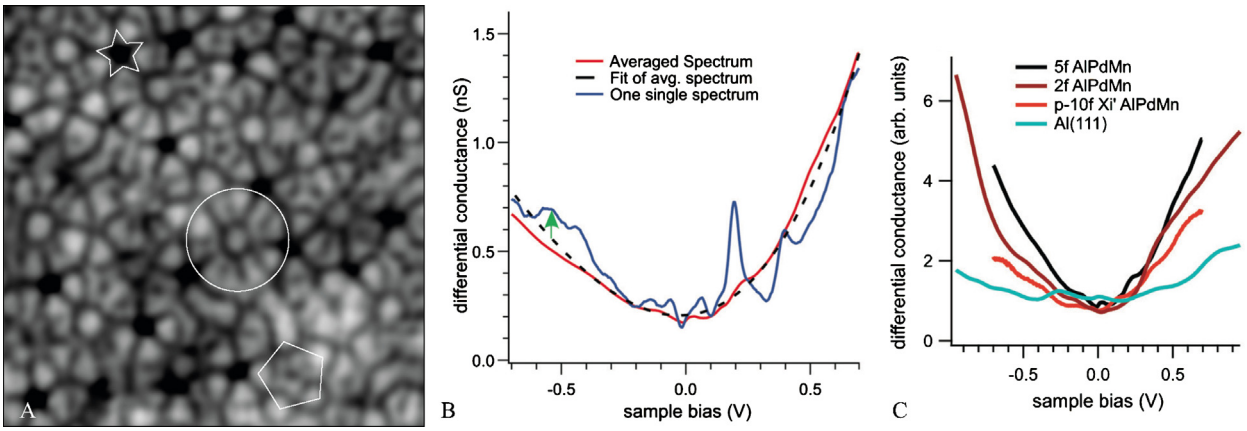

Fig. 2. (a) 10 nm × 10 nm high-resolution STM image obtained on the clean five-fold i-$Al_{70}Pd_{21}Mn_9$ quasicrystal surface. The white flower, dark star and pentagonal tile used to derive the Penrose *P1* tiling have been highlighted. (b) Representative differential conductance dI/dV spectrum (blue line or spiky line) recorded on a quasicrystal surface. A spectrum (red/full line) averaged over 2380 conductance curves along with the fitted average spectrum (dashed line) is also presented. (c) Normalized differential conductance spectra versus bias voltage measured on the Al(111) crystal, pseudo-ten-fold ξ'-Al–Pd–Mn approximant and five- and two-fold Al–Pd–Mn quasicrystal surfaces. (For interpretation of the references to color in this figure legend, the reader is referred to the web version of this article.)
(b–c) from [17], © 2013 by APS.

High-resolution STM images obtained across terraces exhibits several characteristic structural motifs dubbed "dark star" (DS) and "white flower" (WF) (see Fig. 2) that have been found systematically across all terraces [12]. The possible origins of the DS and WF motifs have been thoroughly discussed by Ünal et al. [18]. These features are related to intact and/or truncated Bergman and pseudo-Mackay clusters that are regarded as the basic entities used to build the real-space bulk structure of the icosahedral quasicrystal. Among the different methods used to interpret the atomic arrangement on the i-$Al_{70}Pd_{21}Mn_9$ surface, the connection of points of high contrast has led to the formation of a Penrose *P1* tiling based on rhombuses, pentagonal stars, crowns and regular pentagons [19]. It has been demonstrated that the experimentally derived tiling is contained within the Katz–Gratias–Elser geometric model [20,21]. Moreover, the atomic distribution of the available model has been shown to perfectly reproduce details present on high-resolution STM images. These observations have demonstrated that the topmost surface terminations are Al-rich and that the 6-dimensional polyhedral models could be used to describe the quasicrystalline atomic configurations [22]. These combined results provided direct confirmation in real space that the five-fold i-$Al_{70}Pd_{21}Mn_9$ surface was indeed bulk terminated, as previously suggested by Gierer et al. based on dynamical LEED analysis [23]. In this latter work, the results indicated a bulk-terminated surface with the topmost layer being Al-rich and the layer 0.38 Å beneath having an $Al_{50}Pd_{50}$ composition [23].

Further analysis on the five-fold i-$Al_{70}Pd_{21}Mn_9$ surface has led to a *maximum density rule*[1] for bulk terminations of quasicrystals [24]. This rule not only explained the highest stability of surfaces perpendicular to the five-fold axes at the expense of planes orthogonal to the two-fold axes, but resulted in the modification of the Bravais rule[2] [25]. For quasicrystal surfaces, Bravais' rule still holds if one replaces the concept of single geometrical plane by that of layer of stacked atoms [24]. Finally, along the five-fold direction of the i-$Al_{70}Pd_{21}Mn_9$ quasicrystal, the structure can be described as blocks of atomic layers separated by interlayer spacings (gaps) of various widths and distributed according to the Fibonacci sequence. Combining the above information along with a careful analysis of the step height distribution across several samples, it has been suggested that quasicrystal surfaces arise from bulk truncation at large gaps above regions of relatively large atomic density and high Al content [26].

Regarding the electronic structure of the five-fold i-$Al_{70}Pd_{21}Mn_9$ surface, several studies have been performed to determine the electronic density of states (DOS) near the Fermi level (E_F). Using high-resolution photoemission spectroscopy, it has been shown that the valence band region of the i-$Al_{70}Pd_{21}Mn_9$ sample exhibits a clear Fermi edge along with a lower spectral intensity at E_F within the temperature range investigated [27]. While the former feature indicates a metallic character of the alloy, the second observation is consistent with the existence of the Hume–Rothery pseudogap in the DOS close to E_F, also supported by electronic structure calculations [28,29]. Simultaneously, the investigation of the i-$Al_{70}Pd_{21}Mn_9$ surface using X-ray photoelectron spectroscopy (XPS) has highlighted a large binding energy shift for the Pd 3*d* core level compared to pure Pd and an increased sharpness of Mn 2*p* line in the quasicrystal. The analysis of the Mn line shape using the Doniach–Sunjic fitting procedure indicates a reduced asymmetric parameter compared to a crystalline sample or Mn pure metal [30]. The asymmetry in the transition metal core level line shape is related to the intrinsic loss of the kinetic energy of photoelectrons via electron–hole excitations across the Fermi edge. The probability of such excitation process decays

[1] The most stable surface terminations should not be planes with the highest density, but layers (more than one plane) having the highest density.
[2] It states that the most stable surfaces are those parallel to the densest atomic planes in the bulk.

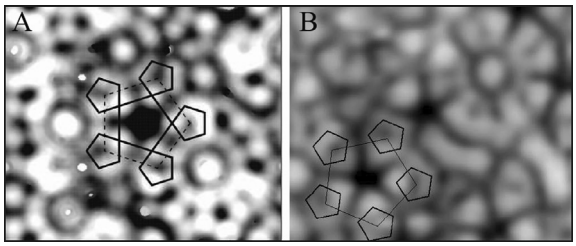

Fig. 3. (a–b) Calculated and experimental STM images of the 3/2 approximant and the five-fold i-$Al_{70}Pd_{21}Mn_9$ surfaces (39.5 Å × 32.9 Å). These constant current images have been obtained at +0.37 V, i.e. contributions of the unoccupied states above the Fermi level. The DS motif consists of a central Al pentagon of edge length 4.79 Å surrounded by five smaller pentagons of edge length 2.96 Å. The dashed large pentagons (edge length 7.8 Å) correspond to the tile used to derive a Penrose *P1* tiling [34].
(a–b) from [34], © 2006 by APS.

rapidly with the electron-hole pair energy and varies with the number of available electronic states close to E_F. While an indirect method, the analysis of the asymmetric shape of the Mn 2*p* core level lines by XPS measurements has demonstrated that the pseudogap present in the bulk is preserved up to the topmost i-$Al_{70}Pd_{21}Mn_9$ surface (five- and three-fold) when prepared by sputter/anneal cycles and vanishes for cleaved surfaces [31]. More recently, scanning tunneling spectroscopy (STS) measurements performed on the five-fold surface at low temperature have revealed local tunneling spectra characterized by narrow peaks and pseudo gaps of energy width ranging from 20 to 50 meV (see Fig. 2b). Interestingly, these features are spatially localized to very small regions of the surface with a spatial extent of about 0.5 to 1 nm [17,32]. The local spikiness of the spectra is well reproduced by tight-binding calculations carried out on a finite patch of the Penrose tiling [32]. A parameter $\hat{S}$ has been introduced to quantify the spatial variability of STS spectra (i.e. the degree of spikiness) and it reflects the localization of electronic states [17]. STS measurements performed on a series of approximants, quasicrystals, and pure metal demonstrate a square-root dependence of the electrical resistivity with the $\hat{S}$ parameter in accordance with previous theoretical works [33]. At low temperatures, the spiky aspect of the local DOS is smeared out if the tunneling spectra are averaged over a larger surface area (see Fig. 2c). The resulting spectrum exhibits the expected large parabolic pseudogap with a sharp and deep dip at E_F (referred to as the zero-bias anomaly).

Following these experimental reports, *ab initio* calculations based on density functional theory (DFT) have been performed to determine the electronic properties, structure, and stability of the i-$Al_{70}Pd_{21}Mn_9$ surface. To performe such calculations, the use of an icosahedral approximant (periodic) has been introduced to model the quasicrystal surface [35]. The atomic arrangement on this approximant can be analyzed using similar Penrose *P1* tiling. Upon relaxation, transition metal elements retain their initial positions while a higher mobility is observed for Al atoms (around the centre of pseudo-Mackay clusters, for instance). The analysis of the surface electron density demonstrates local minima at the *P1* vertices (most of them decorated by Pd) along with strong charge depletions in several pentagonal tiles originating from surface vacancies [35]. A comparison between simulated and experimental STM images (see Fig. 3) has shed some light on the possible origin of the quasicrystal characteristics motifs. The WF feature can be built from an equatorially truncated pseudo-Mackay cluster surrounded by five Bergman clusters (the flower "leaves"). The existence of DS motifs can be assigned to surface vacancies that exist inside several pseudo-Mackay entities [34]. From this study, it is clear that STM images are dominated by Al atoms, while Pd atoms manifest themselves as dark spots. This low contribution is attributed to the low density of Pd states at E_F, to the localized character of Pd *d* states compared to Al *s, p* states and to its location 0.48 Å below the topmost surface plane. The bright contrast associated with Mn atoms (central part of the WF motifs, for instance) is explained by a low coordination leading to a very low width of the Mn *d* band [34]. This work demonstrates that approximant systems can indeed be used to reproduce in minute details the local atomic arrangement on quasicrystal surfaces. It also reinforces the validity of the different rules established to generate the terminations at the five-fold i-$Al_{70}Pd_{21}Mn_9$ surface.

2.2. The five-fold surface of the icosahedral Ag–In–Yb quasicrystal

The discovery of a stable binary i-Cd–Yb (Tsai-type) quasicrystal [36] has opened up a new landscape in the community working on aperiodic systems. While the presence of Cd elements prohibited its preparation under ultra-high-vacuum (UHV) conditions (high vapor pressure), this obstacle was circumvented with the discovery of i-Ag–In–Yb, quasicrystal isostructural to i-$Cd_{5.7}Yb$ [37]. To date, there is only one report on the five-fold surface of the i-Ag–In–Yb quasicrystal. After several sputtering and annealing cycles, three main step heights appear at the surface, with the smallest one being the most frequently observed across terraces. A careful analysis of the bias-dependent STM images indicates that surface layers terminate at bulk planes intersecting the centre of rhombic triacontahedral (RTH) clusters, basic building block of the Cd–Yb family [38]. If the surface layers were coinciding with every high density layers present in the bulk model, then only one step height should be observed at the i-Ag–In–Yb quasicrystal surface. The contrast variation in the STM images upon inversion of the bias (occupied or unoccupied electronic states) is also in agreement with the chemical decoration of the RTH clusters.

It is now well accepted that Al-based quasicrystals are stabilized by the Hume–Rothery mechanism combined with *sp–d* hybridization. However, the cohesion of Cd-based compounds originates primarily from *p–d* hybridization, the Hume–Rothery mechanism not playing the principal role in the stability [39,40]. Valence-band structure investigations have been

performed on the two-, three- and five-fold surfaces of the *i*-Ag–In–Yb quasicrystal [41]. As for the cleaved *i*-Cd–Yb quasicrystal [40], comparable surface core-level shifts have been observed for Yb 4f-derived states for all three surface orientations [41]. As foreseen by electronic structure calculations, the Fermi level (E_F) is dominated by the Yb 4f-derived states. In agreement with previous works [39,40], this study further demonstrates that the pseudogap located slightly above E_F originates from the hybridization of the Yb 5*d* band with the Ag and In 5*p* bands.

During the sample growth, it has been found that the cooling rate has a major impact on the structural quality of the resulting *i*-$Ag_{42}In_{42}Yb_{16}$ domains. In addition, for the sample growth conditions that have been used, two types of periodic structures have been identified with relatively large surface unit mesh; 2.14 nm × 3.08 nm (rectangular cell) and 2.10 nm × 1.50 nm (oblique cell). These values have been compared to 1/1 and 2/1 approximant phases and to less complex phases (e.g. In_4Ag_9, $InAg_3$, $YbAg_{5.4}In_{6.6}$ …). Contrary to the icosahedral Al-based quasicrystals, no match has been found yet [42].

2.3. The Al–Ni–Co decagonal quasicrystal surfaces

Compared to the icosahedral quasicrystal samples, bulk planes are periodically spaced along the ten-fold axis of the *d*-Al–Ni–Co sample. STM measurements carried out on a Co-rich quasicrystal exhibit a unique step height of 2 Å ($c/2$) separating atomically flat terraces. For Ni-rich decagonal system (*d*-$Al_{71.7}Ni_{18.7}Co_{9.6}$) and for the type-I superstructure phase ($Al_{71.8}Ni_{14.8}Co_{13.4}$), there is a tendency toward step doubling [43,44]. The ten-fold surface of the *d*-$Al_{73}Ni_{10}Co_{17}$ is completely determined by a single surface layer, which displays a five-fold rotational symmetry. The terminations separated by a single step height are related to each other by a rotation symmetry resulting in ten-fold symmetric low-energy electron diffraction patterns [45]. Using dynamical LEED analysis combined with STM measurements, the structure of this Co-rich surface layer has been determined to be bulk-terminated with a small degree of intralayer rumpling [46]. The surface terminations have the same composition as the bulk. Analysis based on autocorrelation functions resulting from STM images has led to a similar conclusion for the type-I superstructure phase. The fine structure observed on terraces is consistent with bulk-terminated planes. While the structure of the Co-rich surface can be described by a randomized pentagonal Penrose tiling, the type-I superstructure surface is characterized using a random rhombic Penrose tiling [44,46]. Regarding the electronic structure of the decagonal surface, angle-resolved photoemission spectroscopy measurements carried out of the Ni-rich phase indicate strongly dispersing *s*–*p* derived valence states with bands centered at reciprocal lattice points with large structure factor. These free-electron-like bands have been observed on (10000), (00$1\bar{1}$0) and (00001) surfaces, i.e. along both periodic and quasiperiodic directions [47,48].

The structural investigation of two-fold *d*-Al–Ni–Co surfaces has highlighted the occurrence of additional surface phenomena like faceting and/or reconstruction. The inequivalent (12110)[3] and (10000) two-fold surfaces have been studied for different *d*-Al–Ni–Co sample compositions [49–52]. For the *d*-$Al_{70}Ni_{15}Co_{15}$ and *d*-$Al_{72.9}Ni_{10.4}Co_{16.7}$ quasicrystals, (12110) and (10000) surfaces exhibits a columnar structure with respectively a 0.4 nm and 0.8 nm periodicity along the [00001] axis. STM measurements show that the (12110) surface for both sample compositions is faceted into {12110} and {10000} planes [52]. From a thorough analysis of the facet occurrence and width [52], it has been deduced that the surface tension is lower for {10000} than for {12110} planes, as previously suggested from the work performed on the *d*-$Al_{71.8}Ni_{14.8}Co_{13.4}$ (00$1\bar{1}$0) surface [50]. A comparison between STM images and the available bulk model indicates that the (12110) surface termination corresponds to the densest bulk planes having a slightly lower Al concentration than the nominal bulk composition [52]. Terraces are separated by two step heights *L* and *S* distributed aperiodically along the [12110] direction, the L/S ratio approaching the golden mean τ. While the step height sequence and surface chemical composition are comparable for both sample compositions, the structural details of their respective {12110} terraces differ slightly, mainly in the fine column structure (identified as rows of Al dimers within the densest planes of the bulk model) and within the inter-column regions [52]. For the {10000} planes, a similar atomic structure is found for both *d*-$Al_{70}Ni_{15}Co_{15}$ and *d*-$Al_{72.9}Ni_{10.4}Co_{16.7}$ quasicrystals. It is described by two different types of terraces referred as row- and hex-terraces, both displaying a columnar structure of 0.8 nm periodicity along the [00001] directions. From a step height analysis, it appears that the (10000) *d*-Al–Ni–Co surface is best described as a puckered plane, i.e. a thin layer of two bulk planes as previously suggested [24]. The structural motifs observed by STM on the (10000) surface terminations are in agreement with structural units present within the bulk model [52].

3. Artificial two-dimensional quasiperiodic structures

Compared to usual crystals, a quasicrystalline surface as shown in Fig. 2 presents an extremely complex potential energy landscape for adsorption experiments. It was soon realized that if a subset of quasilattice sites act as preferred adsorption sites, then it should be possible to enforce a quasiperiodic structure in the adsorbed film. This would open up the possibility to use aperiodic templates as a new playground to study the relationship that exists between chemical and physical properties and complex surface structure. To this end, one of the challenges has been to determine if and to which extent the surface structure of quasicrystals and approximants could be transferred to thin films made of a single element. This

[3] The (12110) surface is equivalent to the (00$1\bar{1}$0) one.

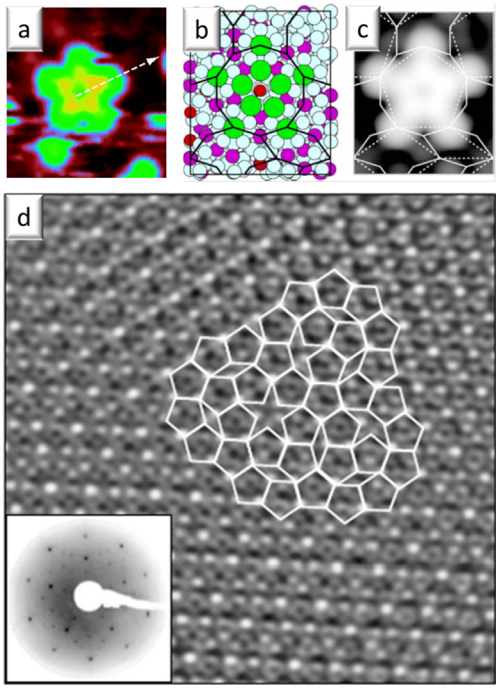

Fig. 4. (Color online.) (a) Experimental STM image of a Pb starfish island. (b and c) Model and calculated STM image of the starfish island. (d) STM image (25 nm × 25 nm) of the completed Pb overlayer on the five-fold surface *i*-Al–Pd–Mn. Inset: LEED pattern recorded at 80 eV at the same coverage. Adapted from Refs. [59,60].

is referred to as a pseudomorphic growth mode. A pseudomorphic monolayer or thin film of reduced chemical complexity might represent an opportunity to evaluate the intrinsic properties associated with aperiodicity. To achieve this objective, several adsorption studies have been carried out on both decagonal and icosahedral surfaces. Aluminium adatoms deposited on the five-fold surface of the *i*-Al–Cu–Fe were found to form small islands with pentagonal shape resembling nanoscale starfish [53]. These islands have all the same orientation with respect to the surface and are presumably made of six adatoms nucleating at specific quasilattice sites identified as DS motifs. The pseudomorphic growth is however limited to a fraction of a monolayer, as these islands do not grow laterally as coverage increases, leading to early roughening of the film.

Local pseudomorphic growth has also been reported at submonolayer coverage for Ag adatoms on the five-fold surface of the *i*-Al–Pd–Mn [54]. Flux and temperature independence of the island density indicated a heterogeneous nucleation of 2D islands at specific sites, also identified as DS sites. With increasing coverage, the 2D islands quickly convert into 3D mesa of specific thickness corresponding to 3-layer-high islands. The mechanism driving the formation of these islands with 'magic height' has been identified with a quantum size effect (QSE). It is induced by electron confinement in the overlayer due to the pseudogap in the DOS at the Fermi level of the quasicrystalline substrate [55,56]. The QSE influence the growth mode of the Ag film to favor islands of selected height. The islands have non-fcc structures in this coverage regime. However, for film thicknesses larger than five monolayers (ML), an fcc structure is recovered with islands having a (111) orientation and five rotational domains rotated by $2\pi/5$ [57]. The first successful growth of a complete pseudomorphic layer was reported by Franke et al. for Bi and Sb films deposited on either the five-fold surface of *i*-Al–Pd–Mn or the ten-fold surface of *d*-Al–Ni–Co. Elastic helium atom scattering and low-energy electron diffraction of the monolayers show Bragg peaks at the bulk derived positions, indicating the formation of highly ordered quasiperiodic epitaxial films [58]. Insight into how the quasiperiodic order is propagated into the films could be obtained on a different system using STM combined with DFT calculations: Pb on the five-fold *i*-Al–Pd–Mn or *i*-Al–Cu–Fe substrates [59–62]. At submonolayer coverage, the growth proceeds by preferential adsorbtion at equatorially truncated pseudo-Mackay clusters present at the surface (WF motifs in Fig. 2a). This leads to the formation of five-fold starfish islands that interconnect to form a 2D quasiperiodic structure as the coverage increases. A comparison of experimental and calculated STM images indicates that the starfish islands are composed of ten Pb atoms, as shown in Fig. 4.

Atomically resolved STM image and LEED patterns of the completed monolayer reveal long-range quasiperiodic order and a high structural quality (see Fig. 4d). The atomic structure of the film can be described by a decorated Penrose *P1* tiling with an edge length which is τ times larger than that of the *P1* tiling used to describe the clean surface (τ is the golden mean). The τ-scaled *P1* tiling connects the centers of the WF motifs of the substrate and thus constitutes the skeleton of the structure of the Pb monolayer. Experimentally, it was found by STS and UPS that the electronic structure of the overlayer is characterized by a deep pseudogap at the Fermi level, which is even more pronounced than that of the clean substrate. The

existence of the pseudogap was reproduced by the calculations and its origin has been ascribed to hybridization between Pb p and substrates states rather than to the quasiperiodic ordering [61]. Also, such quasiperiodic metal overlayers are stabilized by the substrate as they are unstable as freestanding monolayers. Another limitation is the fact that only the first adlayer can be forced to adopt a quasiperiodic structure. The onset of the second layer's growth has not been observed experimentally. It is explained by either the formation of mounds separated by very large distances such that they can hardly be observed by the local probe of the STM or by a reduced Pb sticking coefficient on the quasiperiodic Pb monolayer. It is interesting to note that Pb deposited on an Al (111) surface grow in a layer-by-layer fashion under similar experimental conditions [62]. Thus the non-sticking behavior or the mesoscopic diffusion length of Pb adatoms is a direct consequence of the quasiperiodic nature of the adlayer. An interesting development of this study would be to measure adhesion and friction forces on such a system.

4. Surface-related properties

Over the years, several groups studying tribology, wetting, and reactivity have reported that quasicrystals and approximants exhibit exceptional surface properties [63]. Most of the envisaged industrial applications of these complex intermetallics make use of their surface properties, e.g., non-sticking behavior, oxidation resistance, high hardness, low thermal conductivity, low coefficient of friction, and more recently catalytic activity [64]. Here, we will only recall the recent works related to the last two surface properties.

The anisotropic friction properties between quasiperiodic and periodic systems have been well illustrated by Park et al. using atomic force microscopy. A two-fold decagonal quasicrystal surface has been chosen as it exhibits one periodic and one aperiodic axis perpendicular to each other [65]. The torsional response of the AFM cantilever has been monitored as a function of the scanning angle. The measurements indicate a torsional response along the ten-fold (periodic) direction about eight times higher than along the two-fold (aperiodic) direction. The constant electrical conductance simultaneously recorded during the experiment demonstrates that the contact area has not changed with the directions. For both periodic and aperiodic directions, this friction anisotropy is still preserved when investigating the torsional response of the lever as a function of applied loads throughout the wearless regime [65]. However, it is reduced by half if the surface is exposed to 100 Langmuir of ethylene at room temperature and disappears when the surface is oxidized [64–66]. These observations suggest that the measured anisotropy arises from short-range tip-surface interactions, the latter being more efficiently screened by an oxide than an ethylene layer [66]. The short-range interactions will depend on the atomic ordering on the clean surface [65] which will vary with the scanning direction. To interpret the origin of such a friction anisotropy, several factors ranging from tip-surface incommensurability to surface roughness have been considered. Among them, electronic and/or phononic contributions appear as the most likely explanations to account for the anisotropic friction properties. The kinetic energy could then by dissipated via excitation of electron–hole pairs and/or propagation of phonons [65,66]. The presence of gaps along the quasiperiodic direction within the calculated phonon energy spectrum could inhibit phononic excitation and propagation, hence leading to lower energy dissipation [64–66].

Similarly, the potential of quasicrystals in the field of heterogeneous catalysis has been well recognized from early days [67,68]. The brittleness of quasicrystals, and more generally of complex intermetallic compounds, is clearly an advantage when dealing with catalysis as they can easily be crushed into high-surface area powder [69,70]. Therefore, these materials, which are stable phases up to high temperatures, have serious potential to be used as industrial catalysts. Using gas-phase reaction, Al-based quasicrystalline ultrafine particles have been initially produced with a size $d \leqslant 200$ nm. These particles have been reported to exhibit a high catalytic activity in a methanol decomposing reaction and the lowest reaction initiation temperature [67]. The potential catalytic activity of quasicrystalline materials has been assigned to their content in transition metal elements, reaching between 20 to 30 at.% of a known catalyst (Pd, Cu, Ni, ...). Apart from the oxidation of quasicrystal surfaces, which has been well-documented [71–76], information on the surface reactivity of quasicrystals remains limited. Indeed, molecular adsorption studies on model systems[4] have only been performed for a limited amount of organic molecules [77–79]. From these studies, it appears that the surface reactivity of i-$Al_{70}Pd_{21}Mn_9$ towards small molecules (H_2, CO, or methanol, for instance) is very similar to that of pure Al [68,77], with an exception for iodoalkanes, where the stability of atomic iodine and alkyl fragment to high temperature suggests a more reactive (stronger bonds) quasicrystal surface compared to pure Al [77].

Among the several methods available to prepare catalysts, the leaching technique (corresponding here to the removal of Al element) has been applied to the i-Al–Cu–Fe quasicrystal and other related phases [69,70,80,81]. Aperiodic $Al_{63}Cu_{25}TM_{12}$ (TM = Ru, Os, Fe) samples and periodic Al–Cu–(Fe) systems of various composition have then been tested as catalysts for the steam reforming of methanol [70,80,81]. The results indicate that the i-$Al_{63}Cu_{25}Fe_{12}$ sample exhibits a higher level of activity per unit area than for instance other Al–Cu–TM quasicrystals and β and θ crystalline phases. It is comparable to existing Cu-based catalysts currently used in industry [80]. Improvements of the Al–Cu–Fe catalytic properties have been achieved by varying the milling process (resulting in particles of high surface area), the leaching temperature and aqueous solution [70]. Scanning electron microscopy (SEM) images (see Fig. 5a–b) reveal considerable microstructure differences between the Rayney Cu catalyst and leached quasicrystal surfaces [70], where the former is described as a skeleton of

[4] We understand here the i-$Al_{70}Pd_{21}Mn_9$ and d-Al–Ni–Co surfaces prepared by sputtering and annealing cycles under ultra high vacuum conditions.

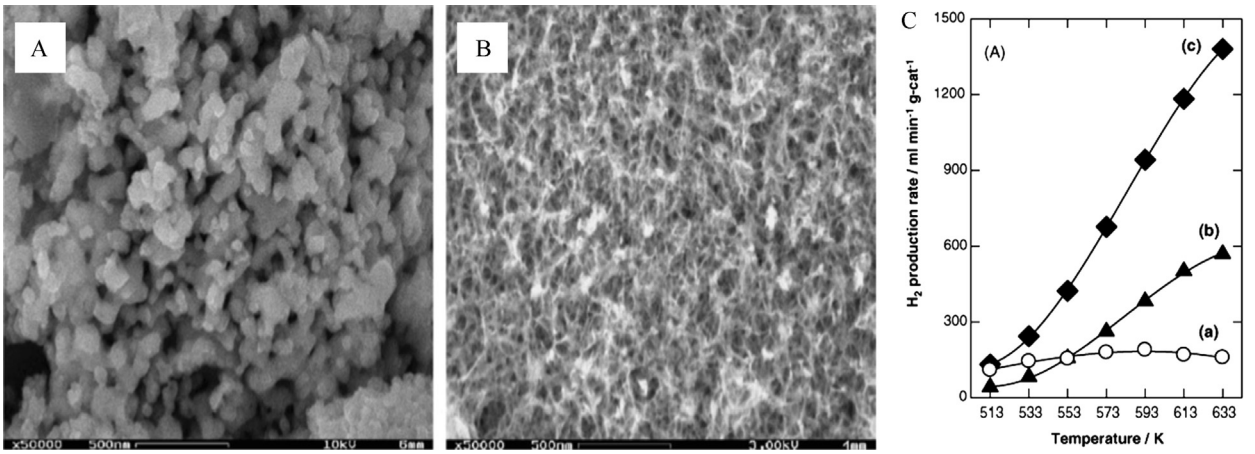

Fig. 5. SEM of (a) Rayney Cu catalyst and (b) *i*-$Al_{63}Cu_{25}Fe_{12}$ quasicrystal (QC) after a leaching treatment in Na_2CO_3 aqueous solution at 298 K. (c) H_2 production rate for SRM versus the reaction temperature for (a) the Rayney Cu catalyst, (b) the QC prepared by dry and (c) wet milling process and leached at 323 K respectively [70].
(a–c) from [70], © 2006 by Elsevier.

aggregated Cu/CuO particles and the latter consists of porous Al oxides. The origin of the catalytic performance of the Al–Cu–Fe quasicrystal (see Fig. 5c) is attributed to highly dispersed and stable Cu species generated by the leaching treatment. Copper particle sintering is inhibited by the presence of Fe and/or Fe oxides [70,81,82]. The interaction between Cu and Fe oxides (both elements being immiscible) are also proposed for the enhanced catalytic performance [82]. Recent studies validate this point and reveal that the high stability and activity of the Al–Cu–Fe quasicrystal originate from the formation of a homogeneous mixture of Cu and Fe oxides in the NaOH leached layer [82]. The microstructure of the leached layer is governed by the Al dissolution rate, which is higher for crystalline alloys compared to quasicrystal compounds. For crystalline samples, the high Al dissolution rate leads initially to a skeletal Cu structure to transform into a Cu-enriched region at the end of the leaching process. For the aperiodic structure, the low dissolution rate is explained by the aperiodic structure of the *i*-$Al_{63}Cu_{25}Fe_{12}$ sample. The Al concentration is layer dependent and it is thought that the leaching process will be reduced when reaching the Al-poor atomic layer [82]. Beneath the leached region, the quasicrystal specimen remains stable upon the catalytic reaction.

This work has been recently extended to periodic systems like the decagonal $Al_{13}TM_4$ (TM = Co, Fe) approximants, which have been identified as hydrogenation catalysts [83]. The $Al_{13}Fe_4$ compound has been proposed as a low-cost alternative to Pd-based industrial catalysts for the semi-hydrogenation of acetylene [84]. The remarkable properties of this compound is thought to rely on particular chemical bonding within the structure, leading to the site isolation concept [85,86]. From the recent structural investigation of the $Al_{13}Fe_4$ (010) surface [87], stable Al_5Fe complex decorating the surface is proposed as catalytically active ensembles, in accordance with theoretical calculations performed on the $Al_{13}Co_4$ (100) surface [88].

5. Conclusions

Clean surfaces can be prepared in UHV conditions, allowing an atomic scale description of their structures. It is established that the surface of Al-based QCs are bulk terminated at specific dense planes. Regarding their electronic structure, the pseudogap characteristic of the bulk appears to be maintained at the surface and this feature necessarily has some influence on the physical and chemical properties of quasicrystalline surfaces. There are also some evidences for the existence of localized electronic states on a length scale comparable to the size of the cluster building blocks. In addition, quasiperiodic surfaces represent a complex potential energy landscape for adsorbates and this leads to unusual phenomena in thin film growth, including quantum size effects, preferred nucleation at specific trap sites, and eventually pseudomorphic growth. Regarding the surface properties, quasiperiodic order is associated with lower friction, as demonstrated by friction anisotropy on two-fold decagonal surfaces. It is also characterized by low adhesion and a higher oxidation resistance. Of current interest is the role of chemical bonding on the surface adsorption properties and its chemical reactivity, with the idea to design new intermetallic compounds for catalysis.

References

[1] A. Garn, D. Levine, Phys. Rev. Lett. 59 (1987) 1683.
[2] C. Beeli, G. Gödecke, R. Lück, Philos. Mag. Lett. 78 (1998) 339.
[3] F. Kluge, M. Yureschko, K. Urban, P. Ebert, Surf. Sci. 519 (2002) 33.
[4] J. Dubois, Useful Quasicrystals, World Scientific, Singapore, 2005.
[5] B. Bolliger, M. Erbudak, D. Vvedensky, M. Zurkirch, A. Kortan, Phys. Rev. Lett. 80 (1998) 5369.
[6] Z. Shen, M. Kramer, C. Jenks, A. Goldman, T. Lograsso, D. Delaney, M. Heinzig, W. Raberg, P. Thiel, Phys. Rev. B 58 (1998) 9961.

[7] B. Bolliger, M. Erbudak, A. Hensch, D. Vvedensky, Mater. Sci. Eng. A 859 (2000) 294–296.
[8] D. Naumović, P. Aebi, L. Schlapbach, C. Beeli, Mater. Sci. Eng. A 294–296 (2000) 882.
[9] B. Bolliger, M. Erbudak, A. Hensch, A. Kortan, D. Vvedensky, Mater. Res. Soc. Symp. Proc. 553 (1999) 257.
[10] J. Ledieu, A. Munz, T. Parker, R. McGrath, R. Diehl, D. Delaney, T. Lograsso, Surf. Sci. 433 (435) (1999) 665.
[11] P. Ebert, F. Yue, K. Urban, Phys. Rev. B 57 (1998) 2821.
[12] Z. Papadopolos, G. Kasner, J. Ledieu, E. Cox, N. Richardson, Q. Chen, R. Diehl, T. Lograsso, A. Ross, R. McGrath, Phys. Rev. B 66 (2002) 184207.
[13] T. Schaub, D. Bürgler, H.-J. Güntherodt, J.-B. Suck, Phys. Rev. Lett. 73 (1994) 1255.
[14] Z. Shen, C. Stoldt, C. Jenks, T. Lograsso, P. Thiel, Phys. Rev. B 60 (1999) 14688.
[15] J. Ledieu, E. Cox, R. McGrath, N. Richardson, Q. Chen, V. Fournée, T. Lograsso, A. Ross, K. Caspersen, B. Unal, J. Evans, P. Thiel, Surf. Sci. 583 (2005) 4.
[16] J. Ledieu, C. Muryn, G. Thornton, R. Diehl, D. Delaney, T. Lograsso, R. McGrath, Surf. Sci. 472 (2000) 89.
[17] R.M.R. Widmer, P. Gröning, W. Steurer, O. Gröning, Phys. Rev. B 87 (2013) 075425.
[18] B. Unal, C. Jenks, P. Thiel, Phys. Rev. B 77 (2008) 195419.
[19] J. Ledieu, R. McGrath, R. Diehl, T. Lograsso, A. Ross, Z. Papadopolos, G. Kasner, Surf. Sci. Lett. 492 (2001) L729.
[20] A. Katz, D. Gratias, in: C. Janot, R. Mosseri (Eds.), Proceedings of the 5th International Conference on Quasicrystals, ICQ-5, World Scientific, Singapore, 1995.
[21] V. Elser, Philos. Mag. 73 (1996) 641.
[22] L. Barbier, D.L. Floc'h, Y. Calvayrac, D. Gratias, Phys. Rev. Lett. 88 (2002) 85506.
[23] M. Gierer, M.V. Hove, A. Goldman, Z. Shen, S.-L. Chang, C. Jenks, C.-M. Zhang, P. Thiel, Phys. Rev. Lett. 78 (1997) 467.
[24] Z. Papadopolos, P. Pleasants, G. Kasner, V. Fournée, C. Jenks, J. Ledieu, R. McGrath, Phys. Rev. B 69 (2004) 224201.
[25] M.A. Bravais, Études cristallographiques, première partie : Du cristal considéré comme un simple assemblage de points. Présenté à l'Académie des sciences, le 26 février 1849 (1849) 168.
[26] H. Sharma, V. Fournée, M. Shimoda, A. Ross, T. Lograsso, A. Tsai, A. Yamamoto, Phys. Rev. Lett. 93 (2004) 165502.
[27] Z. Stadnik, D. Purdie, M. Garnier, Y. Baer, A.-P. Tsai, A. Inoue, K. Edagawa, S. Takeuchi, Phys. Rev. Lett. 77 (1996) 1777.
[28] G.T. de Laissardière, T. Fujiwara, Phys. Rev. B 50 (1994) 5999.
[29] M. Krajčí, M. Windisch, J. Hafner, G. Kresse, M. Mihalkovič, Phys. Rev. B 51 (1995) 17355–17378.
[30] C. Jenks, D. Delaney, T. Bloomer, S.-L. Chang, T. Lograsso, Z. Shen, C.-M. Zhang, P. Thiel, Appl. Surf. Sci. 103 (1996) 485.
[31] V. Fournée, P. Pinhero, J. Anderegg, T. Lograsso, A. Ross, P. Canfield, I. Fisher, P. Thiel, Phys. Rev. B 62 (2000) 14049.
[32] R. Widmer, P. Gröning, M. Feuerbacher, O. Gröning, Phys. Rev. B 79 (2009) 104202.
[33] G.T. de Laissardière, J.-P. Julien, D. Mayou, Phys. Rev. Lett. 97 (2006) 026601.
[34] M. Krajčí, J. Hafner, J. Ledieu, R. McGrath, Phys. Rev. B 73 (2006) 024202.
[35] M. Krajčí, J. Hafner, Phys. Rev. B 71 (2005) 054202.
[36] A. Tsai, J. Guo, E. Abe, H. Takakura, T. Sato, Nature 408 (6812) (2000) 537–538.
[37] J.Q. Guo, A.P. Tsai, Philos. Mag. Lett. 82 (2002) 349.
[38] H. Sharma, M. Shimoda, K. Sagisaka, H. Takakura, J.A. Smerdon, P. Nugent, R. McGrath, D. Fujita, S. Ohhashi, A.P. Tsai, Phys. Rev. B 80 (2009) 121401(R).
[39] Y. Ishii, T. Fujiwara, Phys. Rev. Lett. 87 (2001) 206408.
[40] R. Tamura, T. Takeuchi, C. Aoki, S. Takeuchi, T. Kiss, T. Yokoya, S. Shin, Phys. Rev. Lett. 92 (2004) 146402.
[41] H. Sharma, G. Simutis, V. Dhanak, P. Nugent, C. Cui, M. Shimoda, R. McGrath, A. Tsai, Y. Ishii, Phys. Rev. B 81 (2010) 104205.
[42] H. Sharma, P. Nugent, J. Smerdon, M. Shimoda, S. Ohhashi, V. Fournée, J. Ledieu, A. Tsai, J. Phys. Conf. Ser. 226 (2010) 012004.
[43] H. Sharma, M. Shimoda, A. Tsai, Adv. Phys. 56 (2007) 403.
[44] H. Sharma, K. Franke, W. Theis, A. Riemann, S. Fölsch, P. Gille, K. Rieder, Phys. Rev. B 70 (2004) 235409.
[45] R. Diehl, J. Ledieu, N. Ferralis, A. Szmodis, R. McGrath, J. Phys. Condens. Matter 15 (2003) R1–R19.
[46] N. Ferralis, K. Pussi, E. Cox, M. Gierer, J. Ledieu, I. Fisher, C. Jenks, M. Lindroos, R. McGrath, R. Diehl, Phys. Rev. B 69 (2004) 153404.
[47] E. Rotenberg, W. Theis, K. Horn, P. Gille, Nature 406 (2000) 602.
[48] W. Theis, E. Rotenberg, K. Franke, P. Gille, K. Horn, Phys. Rev. B 68 (2003) 104205.
[49] M. Kishida, T. Kamimura, R. Tamura, K. Edagawa, S. Takeuchi, T. Sato, Y. Yokoyama, J. Guo, A. Tsai, Phys. Rev. B 65 (2002) 94208.
[50] H. Sharma, W. Theis, P. Gille, K. Rieder, Surf. Sci. 511 (2002) 387.
[51] H. Sharma, K. Franke, W. Theis, A. Riemann, S. Fölsch, P. Gille, K. Rieder, Surf. Sci. 561 (2004) 121.
[52] R. Mäder, R. Widmer, P. Gröning, S. Deloudi, W. Steurer, M. Heggen, P. Schall, M. Feuerbacher, O. Gröning, Phys. Rev. B 80 (2009) 035433.
[53] T. Cai, J. Ledieu, R. McGrath, V. Fournée, T. Lograsso, A. Ross, P. Thiel, Surf. Sci. 526 (2003) 115.
[54] B. Ünal, V. Fournée, P. Thiel, J. Evans, Phys. Rev. Lett. 102 (2009) 196103.
[55] V. Fournée, H. Sharma, M. Shimoda, A. Tsai, B. Unal, A. Ross, T. Lograsso, P. Thiel, Phys. Rev. Lett. 95 (2005) 155504.
[56] P. Moras, Y. Weisskopf, J.-N. Longchamp, M. Erbudak, P.H. Zhou, L. Ferrari, C. Carbone, Phys. Rev. B 74 (2006) 121405.
[57] V. Fournée, T. Cai, A. Ross, T. Lograsso, J. Evans, P. Thiel, Phys. Rev. B 67 (2003) 033406.
[58] K. Franke, H. Sharma, W. Theis, P. Gille, P. Ebert, K. Rieder, Phys. Rev. Lett. 89 (2002) 156104.
[59] J. Ledieu, L. Leung, L. Wearing, R. McGrath, T. Lograsso, D. Wu, V. Fournée, Phys. Rev. B 77 (2008) 073409.
[60] J. Ledieu, M. Krajčí, J. Hafner, L. Leung, L. Wearing, R. McGrath, T. Lograsso, D. Wu, V. Fournée, Phys. Rev. B 79 (2009) 245405.
[61] M. Krajčí, J. Hafner, J. Ledieu, V. Fournée, R. McGrath, Phys. Rev. B 82 (2010) 085417.
[62] T. Deniozou, J. Ledieu, V. Fournée, D.M. Wu, T.A. Lograsso, H.I. Li, R.D. Diehl, Phys. Rev. B 79 (2009) 245405.
[63] E. Belin-Ferré (Ed.), Surface Properties and Engineering of Complex Intermetallics, World Scientific, Singapore, 2010.
[64] J.-M. Dubois, E. Belin-Ferré, Complex Metallic Alloys, Wiley–VCH Verlag GmbH & Co., Weinheim, Germany, 2011.
[65] J.Y. Park, D.F. Ogletree, M. Salmeron, R.A. Ribeiro, P.C. Canfield, C.J. Jenks, P.A. Thiel, Science 309 (2005) 1354.
[66] J.Y. Park, D.F. Ogletree, M. Salmeron, R.A. Ribeiro, P.C. Canfield, C.J. Jenks, P.A. Thiel, Phys. Rev. B 74 (2006) 024203.
[67] T. Masumoto, A. Inoue, Y. Corporation, H. Giken, K.K. Kaisha, Eur. Patent 0645464A2, Application number 94115137.5, 26 September 1994.
[68] C. Jenks, P.A. Thiel, J. Mol. Catal. A, Chem. 131 (1998) 301–306.
[69] A.P. Tsai, M. Yoshimura, Appl. Catal. 214 (2001) 237–241.
[70] T. Tanabe, S. Kameoka, A.P. Tsai, Catal. Today 111 (2006) 153–157.
[71] S.-L. Chang, W. Chin, C.-M. Zhang, C. Jenks, P. Thiel, Surf. Sci. 337 (1995) 135.
[72] S.-L. Chang, J. Anderegg, P. Thiel, J. Non-Cryst. Solids 195 (1996) 95.
[73] P. Pinhero, S.-L. Chang, J. Anderegg, P. Thiel, Philos. Mag. B 75 (1997) 271.
[74] C. Jenks, P. Pinhero, S.-L. Chang, J. Anderegg, M. Besser, D. Sordelet, P. Thiel, in: A.I. Goldman, D.J. Sordelet, P.A. Thiel, J.-M. Dubois (Eds.), New Horizons in Quasicrystals: Research and Applications, World Scientific, Singapore, 1997.
[75] S. Suzuki, Y. Waseda, N. Tamura, K. Urban, Scr. Mater. 35 (1996) 891.
[76] D. Rouxel, P. Pigeat, Prog. Surf. Sci. 81 (2006) 488–514.
[77] C. Jenks, T. Lograsso, P. Thiel, J. Am. Chem. Soc. 120 (1998) 12668.

[78] R. McGrath, J. Ledieu, E. Cox, S. Haq, R. Diehl, C. Jenks, I. Fisher, A. Ross, T. Lograsso, J. Alloys Compd. 342 (2002) 432.
[79] J.-T. Hoeft, J. Ledieu, S. Haq, T. Lograsso, A. Ross, R. McGrath, Philos. Mag. 86 (2006) 869.
[80] M. Yoshimura, A.P. Tsai, J. Alloys Compd. 342 (2002) 451–454.
[81] S. Kameoka, A.P. Tsai, Catal. Today 93–95 (2004) 23–26.
[82] T. Tanabe, S. Kameoka, A.P. Tsai, Appl. Catal. A, Gen. 384 (2010) 241–251.
[83] M. Armbrüster, K. Kovnir, Y. Grin, R. Schlögl, P. Gille, M. Heggen, M. Feuerbacher, Ordered cobalt-aluminum and iron-aluminum intermetallic compounds as hydrogenation catalysts, ep09157875.7, 2009.
[84] M. Armbrüster, K. Kovnir, M. Friedrich, D. Teschner, G. Wowsnick, M. Hahne, P. Gille, L. Szentmiklósi, M. Feuerbacher, M. Heggen, F. Girgsdies, D. Rosenthal, R. Schlögl, Y. Grin, Nat. Mater. 11 (2012) 690–693.
[85] Y. Grin, B. Bauer, U. Burkhardt, R. Cardoso-Gil, J. Dolinšek, M. Feuerbacher, P. Gille, F. Haarmann, M. Heggen, P. Jeglič, M. Müller, S. Paschen, W. Schnelle, S. Vrtnik, in: Euromat 2007: European Congress on Advanced Materials and Processes, Nuremberg, Germany, 2007.
[86] K. Kovnir, M. Armbrüster, D. Teschner, T. Venkov, F. Jentoft, A. Knop-Gericke, Y. Grin, R. Schlögl, Sci. Technol. Adv. Mater. 8 (2007) 420.
[87] J. Ledieu, E. Gaudry, L. Serkovic-Loli, S.A. Villaseca, M.-C. de Weerd, M. Hahne, P. Gille, Y. Grin, J.-M. Dubois, V. Fournée, Phys. Rev. Lett. 110 (2013) 076102.
[88] M. Krajčí, J. Hafner, J. Catal. 278 (2011) 200.